J Solid State Electrochem (2012) 16:1493–1502
DOI 10.1007/s10008-011-1548-8

ORIGINAL PAPER

Improved sintering and electrical properties of La-doped CeO_2 buffer layer for intermediate temperature solid oxide fuel cells using doped $LaGaO_3$ film prepared by screen printing process

Jong-Eun Hong · Toru Inagaki · Shintaro Ida · Tatsumi Ishihara

Received: 25 July 2011 / Revised: 1 September 2011 / Accepted: 3 September 2011 / Published online: 2 October 2011

Abstract Effects of a sintering agent for La-doped ceria (LDC) as a buffer layer to prevent a chemical reaction between Ni in anode and Sr- and Mg-doped lanthanum gallate (LSGM) electrolyte during sintering were studied for improving sintering and electrical properties. Electrochemical performance of anode-supported solid oxide fuel cells (SOFCs) using LDC and LSGM films prepared by screen printing and co-sintering (1,350 °C) was also investigated. The prepared cell with dense LDC (ca. 17 μm) and LSGM electrolyte (ca. 60 μm) films showed an open circuit voltage close to the theoretical value of 1.10 V and a high maximum power density (0.831 Wcm^{-2}) at 700 °C. The addition of 1 wt.% LSGM to porous LDC buffer layer was effective for improving the sintering density and electrical conductivity, resulting in the high power density due to the decreased internal resistance loss.

J.-E. Hong · T. Ishihara
Department of Automotive Science, Graduate School of Integrated Frontier Sciences, Kyushu University,
Motooka 744, Nishi-Ku,
Fukuoka 819-0395, Japan

J.-E. Hong (✉) · S. Ida · T. Ishihara
Department of Applied Chemistry, Faculty of Engineering, Kyushu University,
Motooka 744, Nishi-Ku,
Fukuoka 819-0395, Japan
e-mail: hong_je@cstf.kyushu-u.ac.jp

T. Inagaki
Kansai Electric Power Co., Inc.,
11-20 Nakoji 3-chome,
Amagasaki, Hyogo 661-0974, Japan

Keywords Solid oxide fuel cell · $LaGaO_3$ film · La-doped CeO_2 · Sintering agent · Electrical conductivity · Screen printing

Introduction

Solid oxide fuel cells (SOFCs) have been attracting much interest as a reliable and efficient power generator because of their high efficiency. One of the most important objectives in the development of intermediate temperature solid oxide fuel cells (IT-SOFCs) is to increase power density and energy-conversion efficiency at 500–700 °C. Moreover, decrease in the internal resistance of the cell is essential for IT-SOFCs [1–3]. Sr- and Mg-doped lanthanum gallate (LSGM) is considered to be a promising alternative electrolyte material because of its higher oxide ionic conductivity and oxygen transport number [4, 5]. In recent years, there have been many studies on the performance of SOFCs using a thick LSGM electrolyte support [6, 7]. However, the ohmic resistance of the thick electrolyte was still larger than that of the electrodes, although the electrode polarization loss became dominant at 700 °C [7]. Thus, it is expected that further improvement in cell performance can be achieved by an anode-supported SOFC using a thin LSGM electrolyte film, owing to the reduced electrolyte resistance loss.

Recently, anode-supported SOFCs using a LSGM electrolyte film were fabricated using several methods [8–18]. Among various processes for preparing a thin-film electrolyte, a conventional wet process such as screen printing, dip coating or centrifugal deposition is simple, cost effective, and favorable from the viewpoint of commercialization for SOFCs. However, preparation of LSGM thin films by the

conventional wet process is rather difficult because of the reaction between Ni in the anode and the LSGM electrolyte during high-temperature sintering (>1,400 °C) [19, 20]. It has been reported that the chemical reaction can be prevented using a La-doped ceria (LDC) as a buffer layer between the LSGM electrolyte and Ni-based anode [6]. Therefore, it would be possible to fabricate both LSGM electrolyte and LDC buffer layer on Ni-containing anode supports by wet processes followed by co-sintering. However, only a few results have been reported for the cell performance using anode-supported LSGM electrolyte films prepared by the conventional wet process [11, 13–16]. This may be due to the fact that sintering LDC is rather difficult, and its electrical conductivity is lower than that of LSGM [21–25]. Therefore, increasing the property of sintering and conductivity on LDC buffer layer plays an important role in cell performance [11].

For a Gd- or Sm-doped ceria (GDC or SDC), effects of sintering additives have been widely investigated. In particular, a transition metal oxide such as CuO, Co_3O_4, Fe_2O_3, and MnO_2 has been reported to improve sintering and electrical properties for doped ceria [26–32]. However, the influence of sintering property for LDC on the power density of the resulting cell has not been studied in details, although a few results on the effect of co-doping for the electrical conductivity of LDC have reported [22–25]. LDC has to be co-fired with LSGM electrolyte for preventing a chemical reaction. Thus, a transition metal is undesirable as a sintering agent of LDC because a cation diffusion of transition metals into LSGM electrolyte may occur during sintering. This induces a partial electronic conduction in LSGM and deteriorates ionic conductivity as well as cell performance [33, 34]. In this aspect, a sintering agent should be inert against the LSGM electrolyte and also the anode.

In this study, the effect of a sintering agent was investigated to enhance sintering and electrical properties of a LDC buffer layer. Various oxides such as ZrO_2, MgO, In_2O_3, Ga_2O_3, SrO, and LSGM were examined as a sintering aid. The electrochemical performance of SOFCs using LDC/LSGM laminating films prepared by screen printing and co-sintering was also investigated at the intermediate temperature range from 500 °C to 700 °C. In addition, characterization on the sintering property of LSGM electrolyte was carried out for a dense and single phase LSGM electrolyte film co-fired at a reduced temperature of 1,350 °C, which was intended to decrease Ni reactivity.

Experimental

Powder preparation

The powder mixture of a commercial NiO (Wako, 99.99%) and $Sm_{0.2}Ce_{0.8}O_{2-\delta}$ (SDC, Daiichi Kigenso Kagaku Kogyo Co. Ltd., Japan) used as the anode support for SOFCs was pressed into a disk (20 mm in diameter) followed by pre-sintering at 800°C for 2 h. LSGM ($La_{0.9}Sr_{0.1}Ga_{0.8}Mg_{0.2}O_{3-\delta}$) was prepared by a solid-state reaction method. Stoichiometric amounts of La_2O_3 (Kishida, 99.99%), $SrCO_3$ (Rare Metallic, 99.99%), Ga_2O_3 (Wako, 99.99%), and MgO (Wako, 99.9%) powders were ball milled in ethanol for 24 h. After drying, the mixture was calcined at different temperatures (900–1,300 °C) for 6 h and then ground. LDC ($La_{0.4}Ce_{0.6}O_{2-\delta}$) was also prepared by ball milling stoichiometric amounts of La_2O_3 and CeO_2 (Wako, 99.99%) in ethanol and then calcined at 1,350 °C for 6 h to obtain a single phase of LDC with fluorite structure (*Fm-3m*).

Sintering agents (5 wt.%) were added by ball milling a mixture of the prepared LDC powder and the additives in the form of oxide and carbonate in ethanol for 2 h. The additives were MgO, SrO (derived from $SrCO_3$), Ga_2O_3, ZrO_2 (Kishida, 99.9%), In_2O_3 (Kishida, 99.9%), and the LSGM powder prepared above. After drying the composite, it was heated at 800 °C for 2 h and then ground. In addition, either LDC or a sintering agent-added LDC powder was mixed with NiO–SDC anode powder of the same weight ratio by ball milling for 1 h and then fired at 1,350 °C for 5 h to examine the reactivity with Ni.

Sample preparation

Sintering properties of LSGM and LDC were studied for preparing a dense LDC/LSGM laminated film on the NiO-SDC anode substrate prepared by screen printing and co-firing. The LSGM powders calcined at 900–1,300 °C were pressed into disks (20 mm in diameter) and then sintered at 1,350 °C for 5 h; this sintering temperature is the condition for co-firing screen printed samples. LDC and sintering agent added LDCs were also sintered under the same conditions.

The screen printing slurries of LDC and LSGM were prepared by mixing each powder with ethyl cellulose as a binder and isobutyric acid as a solvent. Slurries of the buffer and electrolyte layers were screen printed in regular sequences onto the pre-sintered anode, and the printed samples were then dried in air. The coating thickness was controlled by adjusting the coating time. The coated samples were co-fired at 1,350 °C for 5 h in air. A $Sm_{0.5}Sr_{0.5}CoO_3$ (SSC) as the cathode material was prepared by a modified citric acid method. The cathode electrode was prepared using a slurry-coating method on the prepared LSGM electrolyte film. A reference Pt electrode was also coated close to the cathode and connected with a Pt lead wire by using Pt paste. The cathode and the reference were calcined at 1,100 °C for 0.5 h. Pt meshes covered surfaces of the anode and cathode as current collectors. A molten Pyrex glass was used for sealing the cell.

Characterization

Sintering properties of LSGM and LDC powders were confirmed and adjusted to form a dense coating layer without delamination or cracks. The linear shrinkage percent of LSGM and LDC disks was calculated by the change in diameter before and after sintering. The relative density and porosity were measured by the Archimedes method. The electrical conductivity of buffer layer materials was measured by a dc four-probe method in air.. X-ray diffraction (XRD) using Cu Kα radiation (Rigaku Rint 2500, Japan) was analyzed to determine the phase formation. The power generation property of a single cell using LDC buffer and LSGM electrolyte film prepared by screen printing method was measured by a conventional four-probe method at 500–700 °C. Humidified hydrogen (100 ml min^{-1}, with 3 vol.% H_2O) and oxygen (100 ml min^{-1}) were supplied as the fuel and oxidant, respectively. The anode of the cell was reduced in hydrogen before cell test. Overpotential of the prepared cell was measured using a current interruption method. Microstructure of the cell was studied using a scanning electron microscope (SEM, VE-7800, KEYENCE, Japan)/energy dispersive X-ray spectroscopy (EDX) after the cell test.

Results and discussion

For preparation of a thin-film electrolyte by a wet process on an anode support, a co-sintering process is required for both the film layer and the anode at a high temperature. Thus, the sintering properties of the coating layer materials must be confirmed to prevent delamination or sample bending after sintering.

Figure 1 shows the effect of sintering temperature on the relative density for LSGM and LDC disks. The disks were prepared from LSGM and LDC powders, which were calcined at 1,000 °C and 1,350 °C, respectively, and sintered for 5 h. It is found that the LSGM prepared by the solid-state reaction of ball milling can be dense (~99%) after sintering above 1,300 °C. On the other hand, the LDC is still porous (78.3%) after sintering at 1,400 °C. Therefore, it is difficult to form a dense LDC buffer layer with the LSGM electrolyte after co-sintering. Since the LDC shows a low conductivity compared with that of LSGM [4, 21], a large internal resistance (*IR*) loss is expected for the cell with a porous LDC buffer layer. Therefore, in order to achieve a high power density of the cell using LDC/LSGM layers prepared by a wet process, improving sintering and electrical properties of LDC is essentially requested.

Table 1 summarizes the linear shrinkage of LSGM disks. The disks were prepared with calcined powders treated

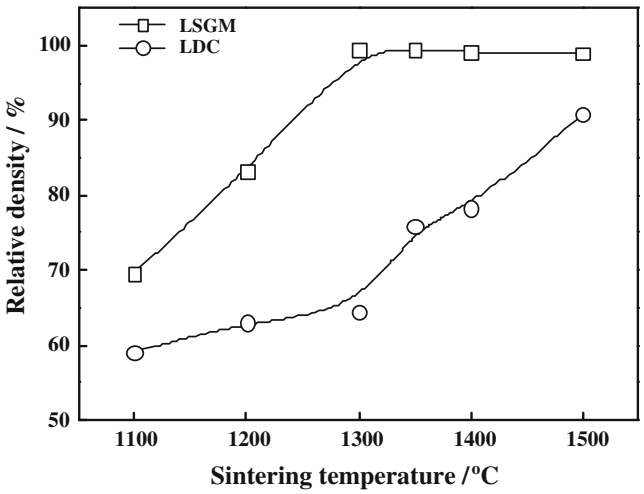

Fig. 1 Relative densities of LSGM and LDC after sintering at various temperatures

under different temperatures after sintering at 1,350 °C. The shrinkage gradually increases with decreasing the calcination temperature of LSGM. This is related to the particle size of the calcined LSGM powder because the powder calcined at lower temperature has a fine particle size. However, the particle size typically increases with increasing calcination temperature and becomes much larger at higher calcination temperatures. Since finer particles have high surface energies, agglomeration and grain growth occur more significantly than in coarse particles during sintering at a given temperature, resulting in a large volumetric change [35]. Similar results with respect to linear shrinkage were also observed for LSGM with different particle sizes-controlled by calcination temperature in this study. Thus, LSGM consisting of fine particles had a much greater shrinkage compared to that calcined at high temperatures.

The effect of LSGM calcination temperature on phase formation was investigated by XRD analysis. Figure 2 shows XRD patterns of LSGM disks prepared from the powders calcined at given temperatures after sintering at 1,350 °C for 5 h. It can be seen that the single phase LSGM with perovskite structure (*Imma*) is obtained by calcination at greater than 900 °C and less than 1,300 °C. However, LSGM calcined at 900 °C and 1,300 °C indicates a secondary phase of $SrLaGaO_4$. Formation of $SrLaGaO_4$ phase is influenced by thermodynamics and solubility of substituted cations in doped $LaGaO_3$ system [36–38]. Rozumek et al. reported that equilibrium phases for LSGM are facilitated by a mass transportation in precursors

Table 1 Linear shrinkage of LSGM disks after sintering at 1350°C as a function of calcination temperature

T (°C)	900	1000	1100	1200	1300
$\Delta L/L$ (%)	20.8	19.7	16.8	15.4	12.4

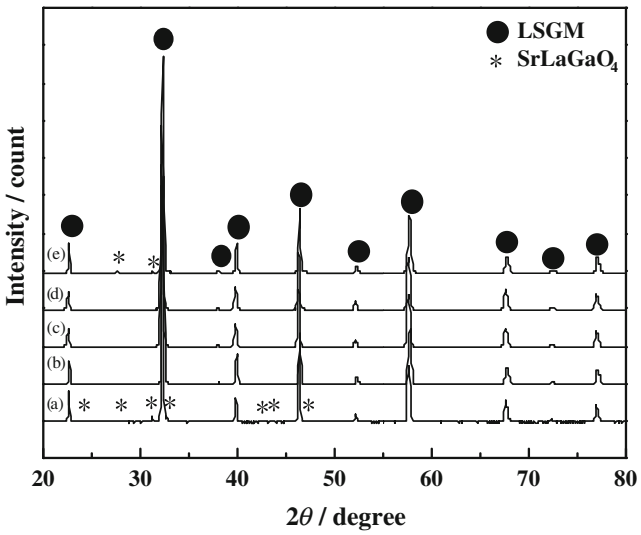

Fig. 2 XRD patterns of LSGM disks after sintering at 1,350 °C as a function of calcination temperature; a 900 °C, **b** 1,000 °C, **c** 1,100 °C, **d** 1,200 °C, and **e** 1300 °C

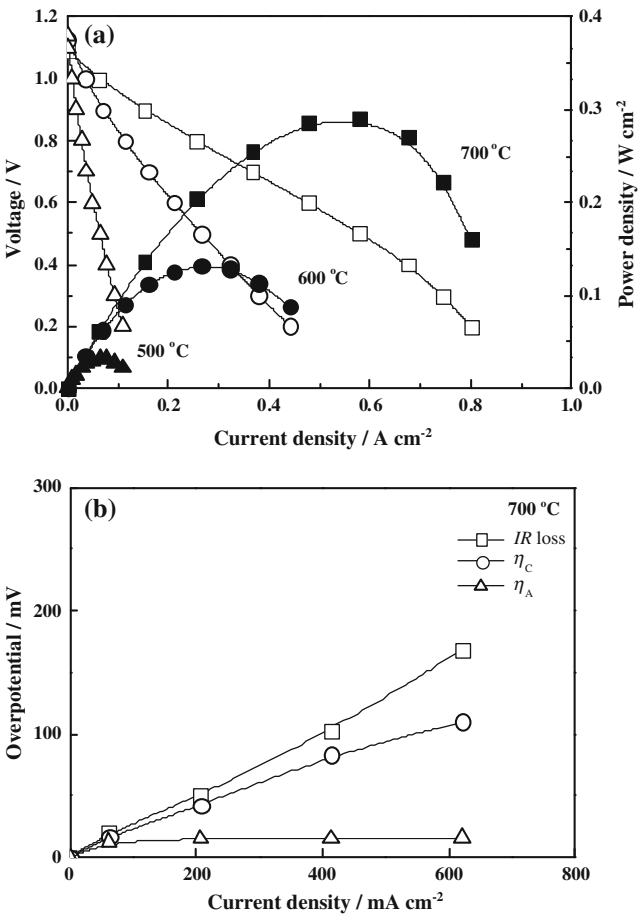

Fig. 3 **a** *I–V* and *I–P* curves and **b** *IR* loss of the cell using LDC buffer and LSGM electrolyte layers. NiO-SDC cermet (Ni/SDC= 60:40) was used for substrate

through an amorphous networking formed with increasing temperatures [37]. In particular, a thermodynamic equilibrium condition is obtained above a certain temperature for LSGM depending on powder preparation methods or compositions. Majewski et al. reported that a liquid phase in a ternary system of SrO–MgO–Ga_2O_3 was observed during DTA measurement. An extended and complete melting was occurred at ~1,260 °C and ~1380 °C, respectively [36]. Thus, the presence of a liquid phase can be also expected during calcination of the LSGM powder. Since the liquid phase during calcination may induce a variation on the stoichiometry of LSGM precursors, this can lead to the formation of secondary phase on the LSGM calcined at 1,300 °C during subsequent sintering. Similarly, the secondary phase of $SrLaGaO_4$ was also detected on the LSGM with the same composition calcined at 1,200 °C followed by 1,400 °C while the final sintering was conducted at 1,500 °C [38]. Accordingly, the dense and pure phase of LSGM perovskite prepared by ball milling is obtained at the temperature range from 900 °C to 1,300 °C for the calcination temperature in this study, although lower sintering temperature was applied.

Figure 3 shows the power generating property of the cell using LDC buffer (ca. 15 μm) and LSGM electrolyte (ca. 60 μm) layers prepared by screen printing followed by co-firing at 1,350 °C. This cell shows 1.09 V of open circuit voltage (OCV) at 700 °C (Fig. 3a), which almost corresponds to the theoretical value of 1.10 V. The OCV substantially increases with decreasing operating temperatures. This suggests that the LSGM electrolyte film prepared by screen printing and co-sintering at 1,350 °C is dense with a negligible gas leakage through the electrolyte. However, maximum power densities (MPDs) are not high as expected from the thickness of LSGM electrolyte (60 μm), i.e., 0.290, 0.132, and 0.032 $W cm^{-2}$ at 700, 600, and 500 °C, respectively. In addition, a rapid drop of the cell voltage was observed at higher current densities probably due to insufficient gas diffusion of the fuel. This cell used a 60 wt.% Ni-SDC cermet which was supposed to have a less porous microstructure for the anode. Figure 3b shows details on the internal resistance of the cell measured by the current interruption method at 700 °C. Evidently, the *IR* loss is dominant for the potential drop of the cell. The estimated *IR* loss is much larger than that of LSGM electrolyte film. Therefore, the large *IR* drop seems to be attributed not to the electrolyte but to the interface or the LDC buffer layer. Considering the low electrical conductivity and porous structure of LDC, one reason for the large *IR* drop can be assigned to the large resistance of the LDC buffer layer. A thinner LDC buffer layer is thus desirable for decreasing the *IR* loss of the cell, but the thinner LDC layer is not suitable for preventing the chemical reaction between the LSGM electrolyte and Ni substrate [11]. Thus, increasing the density and electrical conductivity of the

LDC buffer layer is strongly requested for improving the power generating property of intermediate temperature SOFCs using LSGM electrolyte. Additionally, it should be noted that the cathodic overpotential was also prominent on the cell performance, and it was assumed due to the partial delamination of the SSC cathode layer observed, which might be occurred by the mismatch of thermal expansion coefficient between the LDC/LSGM bi-layer and SSC cathode.

In order to increase the sintering density of the LDC buffer layer, various oxides such as MgO, SrO, ZrO_2, In_2O_3, Ga_2O_3, and LSGM as a sintering aid were examined in this study. Figure 4 shows the SEM images of LDC surfaces with different sintering additives after sintering at 1,350 °C for 5 h. The open porosity is reduced by the addition of SrO, Ga_2O_3, and LSGM (Fig. 4e–g). In particular, much higher sintering density (~99%) is achieved by the addition of LSGM. Since the high density is obtained, and the conductivity of LSGM is higher than that of LDC, it is expected that the electrical conductivity of LDC may be also increased by the LSGM addition. Although the addition of LSGM was effective for improving the sintering density, LSGM addition in the LDC buffer layer would cause a problem of the reaction with Ni in the anode during the co-sintering. However, an effect of LSGM as a sintering agent for LDC has not been reported up to now. Thus, further detailed investigation on the effect of LSGM is needed for optimizing the LSGM sintering agent and increasing the electrical conductivity of the LDC buffer layer.

Figure 5 shows the result on the sintering properties of LDC with different LSGM amounts after sintering at

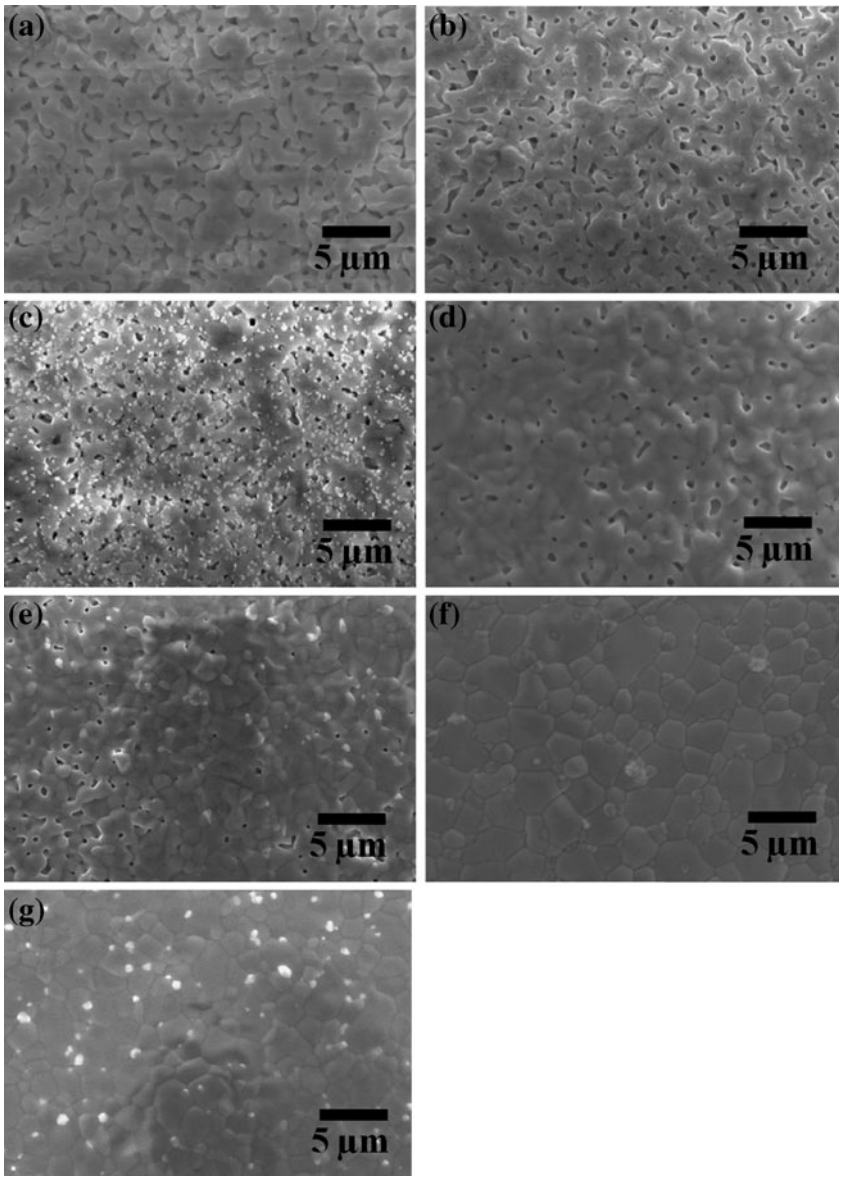

Fig. 4 SEM images of LDCs with and without sintering additives after sintering at 1,350 °C; LDC **a** without additive and with **b** ZrO_2, **c** MgO, **d** In_2O_3, **e** Ga_2O_3, **f** SrO, and **g** LSGM additives

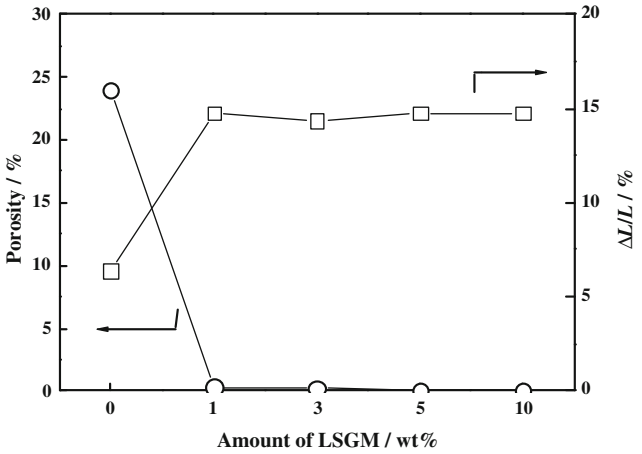

Fig. 5 Effects of LSGM amount in LDC on porosity and linear shrinkage

1,350 °C. The porosity is significantly decreased even adding 1 wt.% LSGM. The shrinkage is also much increased and becomes more compatible with that of LSGM electrolyte (Table 1) by the addition of LSGM sintering aid. This suggests that the small amount of LSGM addition is still effective for enhancing the sintering properties of LDC. Therefore, it is expected that the LDC buffer layer mixed with 1 wt.% LSGM agent could be dense and co-fired with the LSGM electrolyte prepared by screen printing.

Figure 6 shows SEM images on the surfaces of LDCs mixing with different amount of LSGM additives. It was found that large open pores were located on the surface of LDC after sintering (Fig. 4a). In contrast, LSGM added LDCs clearly exhibit much denser and larger grain sized surfaces compared with that of LDC. The grain size of LSGM-LDC rarely varied with the amount of LSGM addition. However, the grain size of LSGM sintering additive placed at grain boundaries or triple junctions in 10 wt.% LSGM-LDC sample is larger than that in 1 wt.% LSGM-LDC, as shown in Fig. 6a and d. The grain size of LSGM particles tends to decrease with reducing the LSGM amount. This implies that the added LSGM particles with the perovskite structure are separated from LDC phase with the fluorite structure and thus segregated at the grain boundaries or triple junctions of LDC during sintering. Moreover, the LSGM addition is supposed to be useful for decreasing the particle size of LDC during ball mill mixing because LSGM particle is smaller than that of LDC. Thus, the linear shrinkage might be also increased by the LSGM addition as small as 1 wt.% along with the densification of the porous LDC.

The effects of the LSGM amount on the phase purity as well as the reactivity against Ni were further studied. Figure 7 shows XRD patterns of LSGM-LDC disks after sintering at 1,350 °C. Main diffraction peaks are assigned to those from the LDC fluorite phase, and perovskite LSGM peaks are substantially detected except for the 1 wt.% LSGM-LDC. There is no impurity peak observed after sintering. This supports that LDC has no reactivity with LSGM [6]. On the other hand, no XRD peak from the LSGM perovskite is observed near $2\theta=40°$ on the sample of 1 wt.% LSGM-LDC. Thus, it was assumed that the amount of LSGM was too small to be detected by XRD measurement. Considering the small amount of LSGM, which is desirable for preventing the reaction with Ni, the optimum amount of LSGM addition for the LDC buffer layer seems 1 wt.%.

Further investigation on the reactivity between 1 wt.% LSGM-LDC and NiO-SDC anode was carried out by powder XRD analysis. As shown in Fig. 8, diffraction peaks assigned only to NiO and doped CeO_2 with the

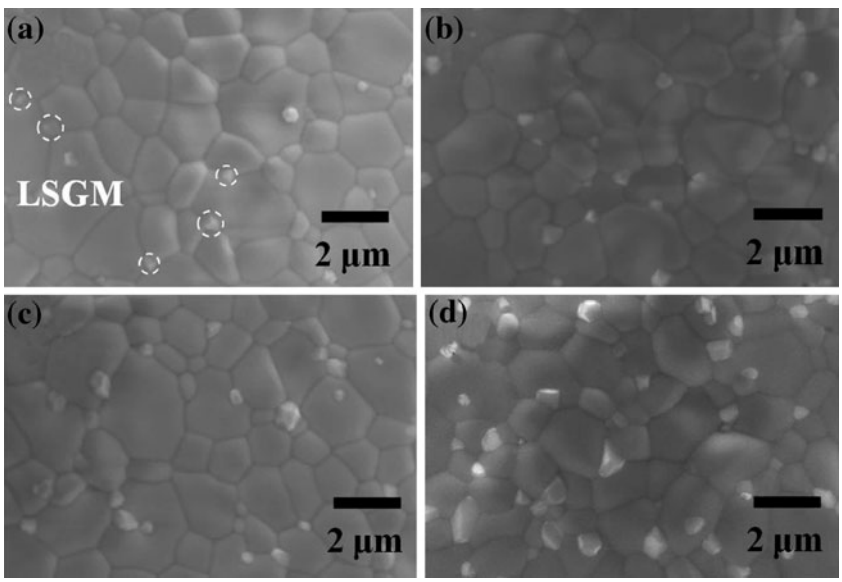

Fig. 6 SEM images of LDCs with different amounts of LSGM additives: **a** 1 wt.%, **b** 3 wt.%, **c** 5 wt.%, and **d** 10 wt.% LSGM

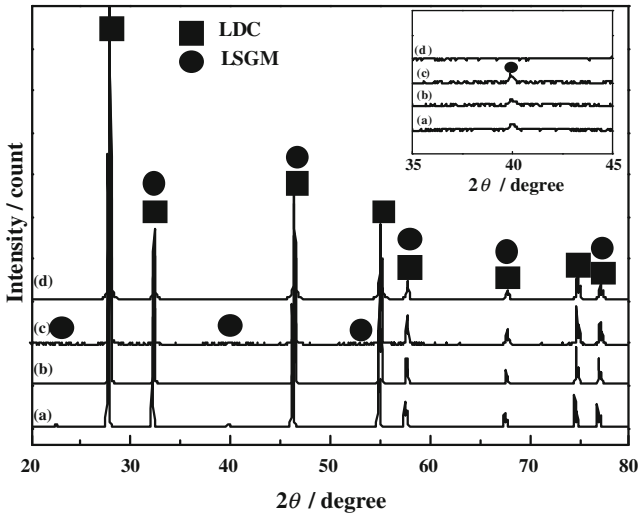

Fig. 7 Comparison of XRD patterns of LDCs with **a** 10 wt.%, **b** 5 wt.%, **c** 3 wt.%, and **d** 1 wt.% LSGM. *Inset* the magnified peaks at $2\theta=40°$

fluorite phase, respectively, are observed in the patterns for the powder mixture of the NiO-SDC and LDC after sintering at 1,350 °C for 5 h. Thus, it reveals that LDC has no reactivity with the anode during sintering. Moreover, XRD peaks for the mixture of the NiO-SDC and 1 wt.% LSGM-LDC (Fig. 8b) are identical to those of the anode and LDC mixture (Fig. 8a). There is neither an impurity phase nor a peak shift observed. This means that the reaction between the anode and 1 wt.% LSGM as a sintering agent in LDC is not recognized. So, it can be said that the influence of 1 wt.% LSGM on the reactivity with Ni is much small enough to be negligible during the sintering. Therefore, it was confirmed that 1 wt.% LSGM had no significant effect or reactivity against the LDC and anode.

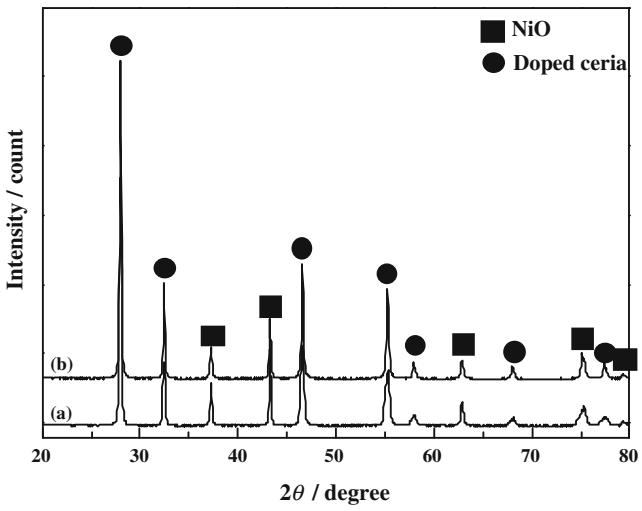

Fig. 8 Comparison of XRD patterns of the powder mixtures of **a** NiO-SDC/LDC and **b** NiO-SDC/1 wt.% LSGM-LDC, sintered at 1,350 °C for 5 h

Influence of the LSGM additive on the conductivity of the LDC material was evaluated. The electrical conductivity for LDC and 1 wt.% LSGM-LDC samples sintered at 1,350 °C for 5 h was measured using a dc four-probe method in air and compared. The Arrhenius representation of the specimens is shown in Fig. 9. The corresponding activation energies were calculated from the slops. It is clear that the conductivity of LDC increases with the addition of LSGM. The measured conductivity of the 1 wt.% LSGM-LDC is 0.010 S cm^{-1} at 700 °C, which is much higher than 0.006 S cm^{-1} of LDC. This value is slightly higher that of a 15 mol% La-doped ceria sintered higher than 1,400 °C [21] but still lower than that of LSGM [4]. In contrast, the activation energy of 1 wt.% LSGM-LDC is not much different compared with that of LDC, as shown in Fig. 9. This suggests that no significant reaction between the LDC and LSGM sintering aid has occurred as confirmed by XRD analysis (Fig. 7). It is noted that in a doped ceria, the electrical transport property is influenced by sintering density and phase homogeneity for bulk transport and also grain size for grain boundary property [39]. Since the 1 wt.% LSGM indicates no chemical interaction with LDC, the possibility related with a phase transformation can be excluded. Therefore, the increased electrical conductivity can be elucidated by the densification and probably a consequent grain growth derived from the LSGM addition. It is thus anticipated that the enhanced conductivity of LDC can be effective for decreasing *IR* loss and thus increasing the power density of the cell using LDC/LSGM screen printed layers.

The electrochemical performance of the single cell using 1 wt.% LSGM-LDC buffer (ca. 17 μm) and LSGM electrolyte (ca. 60 μm) films fabricated by screen printing and co-sintering at 1,350 °C is shown in Fig. 10. LSGM calcined at 1,100 °C was used for the electrolyte layer, and 75 wt.% Ni-SDC cermet anode was used to diminish the

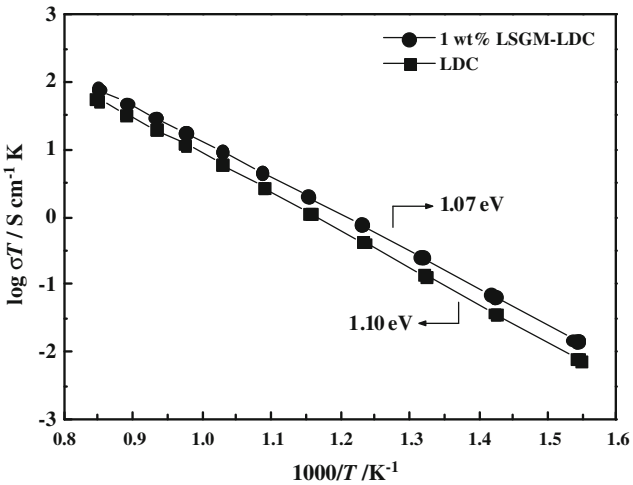

Fig. 9 Temperature dependence of electrical conductivities for LDC and 1 wt.% LSGM-LDC

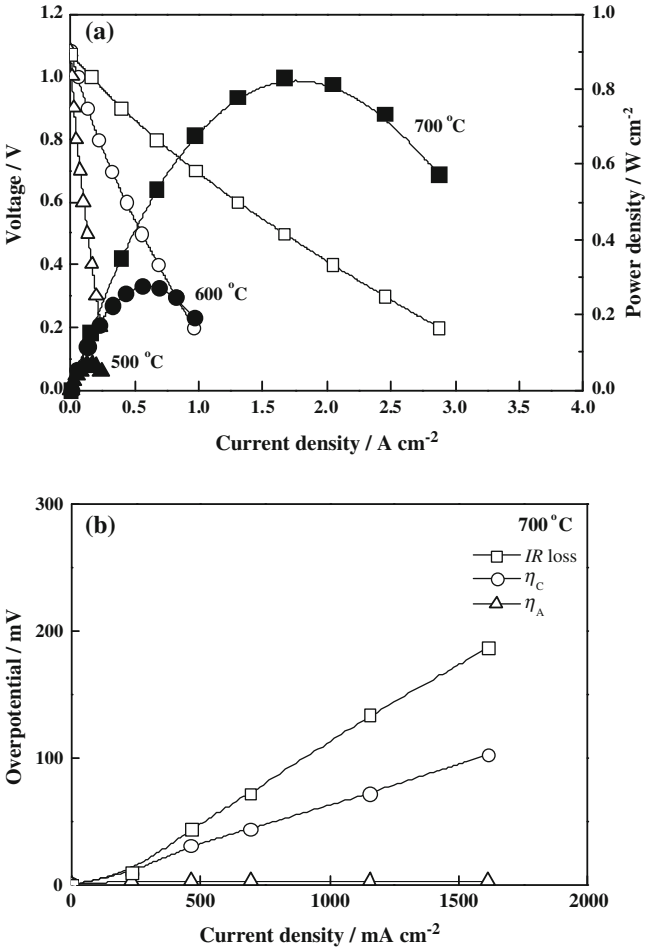

Fig. 10 **a** *I–V* and *I–P* curves and **b** *IR* loss of the cell using 1 wt.% LSGM-LDC buffer and LSGM electrolyte layers. NiO-SDC cermet (Ni/SDC=75:25) was used for substrate

rapid potential drop. This cell shows 1.07 V of the OCV at 700 °C, which is close to the theoretical value. This means that the prepared LSGM electrolyte film is dense, and the screen printing method is reproducible for fabricating the dense LSGM film. Comparing with the result of the cell using the LDC layer (Fig. 3a), this cell shows much improved cell performance. The maximum power densities of 0.831, 0.267, and 0.067 Wcm^{-2} are achieved on the cell at 700 °C, 600 °C, and 500 °C, respectively (Fig. 10a). It should be noted that the observed OCV and MPD are higher than previous data [9, 13–16]. This implies that a high performance can be obtained with an anode-supported SOFC using the 1 wt.% LSGM-LDC buffer and LSGM electrolyte films prepared by screen printing, and the buffer layer effectively works for preventing the formation of a resistive phase between the anode and the LSGM electrolyte film. Figure 10b shows details of the potential drop on the cell. Although the main reason for the overpotential is still the *IR* loss, it is much smaller than that using the LDC buffer layer. *IR* loss can be generally related to two aspects: the electrical resistance of cell components and the contact resistance of electrode/electrolyte. Figure 11 shows the cross-sectional images of the prepared cells using LDC and 1 wt.% LSGM-LDC buffer layer as well as the result of EDX linear analysis on the cell with 1 wt.% LSGM-LDC buffer layer after test. LDC/LSGM and 1 wt.% LSGM-LDC/LSGM layers show good adhesion with the anode, respectively. However, the microstructure of coating layers is much different. The LDC buffer layer is relatively porous compared to the dense 1 wt.% LSGM-LDC layer. Thus, it was confirmed that the sintering density of the LDC buffer layer prepared by screen printing was also enhanced by the addition of 1 wt.% LSGM.

Since a small contact resistance is expected due to the good contact, the difference of the *IR* loss on the cells can be explained by the decreased resistivity of the dense 1 wt.% LSGM-LDC buffer layer. This is why the MPD of the cell using 1 wt % LSGM-LDC layer increases over twice higher than that with the porous LDC layer. On the other hand, the cathodic overpotential on this cell is still large except for the *IR* loss although it is decreased compared with that of the cell in Fig. 3. At present, although the reason for the decreased cathodic overpotential is not clear, it can be related with the improved contact at the interface of the LSGM and SSC layers. This may be related with the

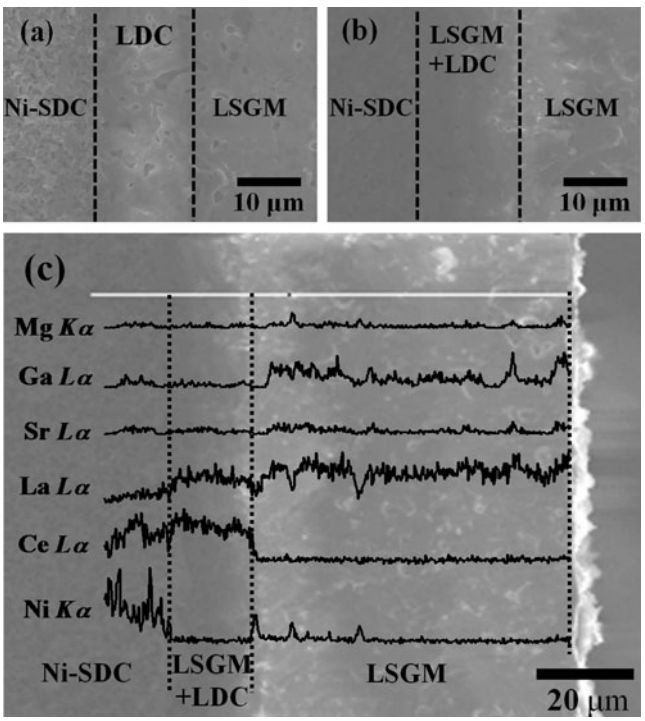

Fig. 11 Cross-sectional SEM images of the cells using **a** LDC/LSGM and **b** 1 wt.% LSGM-LDC/LSGM layers and **c** EDX linear scans on the cross-section of the cell with 1 wt.% LSGM-LDC/LSGM layer after cell test

variation in thermal expansion property of the bi-layer of LSGM and 1 wt.% LSGM-LDC as mentioned in Fig. 5. In any case, the cell performance could be further improved by decreasing the cathodic overpotential. In addition, the lowered anodic overpotential may also have an effect on the cell performance because of the minimized concentration polarization of the anode in Fig. 10. Accordingly, it can be deduced that the electrochemical performance of the cell using the 1 wt.% LSGM-LDC buffer and LSGM electrolyte films is enhanced mainly by the high densification and conductivity of the buffer layer, which is attributed to the LSGM addition in LDC, as well as by the additional reduction of the electrode overpotential. From Fig. 11c, the Ni element was clearly detected at the interface of the 1 wt. % LSGM-LDC and LSGM layers as well as in the LSGM layer. This was also confirmed in the cell using the LDC/ LSGM films. Similar Ni diffusion in a SOFC using a LDC buffer layer with a LSGM electrolyte film prepared by a wet process was reported in other studies [11, 15]. Therefore, it seems that the buffer layer with ~17 μm thickness cannot entirely prevent Ni diffusion during co-firing, although the dense buffer layer can be obtained at the reduced co-sintering temperature. This also implies that the reduced sintering temperature is not enough to inhibit the Ni diffusion. In addition, the Ni remained in the LSGM electrolyte can cause the electronic conduction [40]. Thus, the reduced OCV is attributed to the diffused Ni toward the electrolyte.

Conclusions

Anode-supported SOFCs incorporating a LDC buffer layer and LSGM electrolyte film on a NiO-SDC anode were successfully prepared by screen printing and co-sintering method. A dense LSGM electrolyte with a single perovskite phase was obtained after sintering at 1,350 °C for 5 h. A dense and uniform LDC buffer layer could be also prepared by adding a small amount of LSGM as a sintering agent. The addition of 1 wt.% LSGM improved the sintering density and conductivity of LDC with no significant reactivity with LDC and the anode. MPDs of 0.831, 0.267, and 0.067 Wcm^{-2} on the cell using the 1 wt.% LSGM-LDC buffer and LSGM electrolyte layers were achieved at 700 °C, 600 °C, and 500 °C, respectively, but were slightly lower than that expected from the electrolyte thickness. The reason is supposed due to the still high resistivity of the 1 wt.% LSGM-LDC compared with that of LSGM and the thicker electrolyte film. Ni diffused into the LSGM electrolyte layer, although the dense LDC buffer layer was fabricated at the reduced sintering temperature of 1,350 °C. Accordingly, this study reveals that a LSGM film prepared by screen printing can be used as the electrolyte of intermediate temperature SOFCs with almost theoretical OCV and high power generating property. Sintering and electrical properties of a LDC buffer layer can be improved by the addition of a sintering agent, resulting in decreasing *IR* loss and thus enhancing cell performance.

References

1. Minh NQ (1993) J Am Ceram Soc 76:563–588
2. Hibino T, Hashimoto A, Inoue T, Tokuno J, Yoshida S, Sano M (2000) Science 288:2031–2033
3. Shao Z, Kwak C, Haile SM (2004) Solid State Ionics 175:39–46
4. Ishihara T, Matsuda H, Takita Y (1994) J Am Chem Soc 116:3801–3803
5. Feng M, Goodenough JB (1994) Eur J Solid State Inorg Chem 31:663–672
6. Huang K, Wan JH, Goodenough JB (2001) J Electrochem Soc 148:A788–A794
7. Wan JH, Yan JQ, Goodenough JB (2005) J Electrochem Soc 152: A1511–A1515
8. Yan JW, Lu ZG, Jiang Y, Dong YL, Yu CY, Li WZ (2002) J Electrochem Soc 149:A1132–A1135
9. Bi ZH, Yi BL, Wang ZW, Dong YL, Wu HJ, She YC, Cheng MJ (2004) Electrochem Solid State Lett 7:A105–A107
10. Yan JW, Matsumoto H, Enoki M, Ishihara T (2005) Electrochem Solid State Lett 8:A389–A391
11. Lin YB, Barnett SA (2006) Electrochem Solid State Lett 9:A285–A288
12. Ishihara T, Yan JW, Shinagawa M, Matsumoto H (2006) Electrochim Acta 52:1645–1650
13. He T, He Q, Pei L, Ji Y (2006) J Am Ceram Soc 89:2664–2667
14. Lee DY, Han JH, Kim EG, Song RH, Shin DR (2008) J Power Sourc 185:207–211
15. Guo W, Liu J, Zhang Y (2008) Electrochim Acta 53:4420–4427
16. Bozza F, Polini R, Traversa E (2009) Electrochem Commun 11:1680–1683
17. Ju YW, Eto H, Inagaki T, Ida S, Ishihara T (2010) J Power Sourc 195:6294–6300
18. Ishihara T, Eto H, Yan JW (2011) Int J Hydrogen Energ 36:1862–1867
19. Huang KQ, Feng M, Goodenough JB, Milliken C (1997) J Electrochem Soc 144:3620–3624
20. Hrovat M, Ahmad-Khanlou A, Samardzija Z, Holc J (1999) Mater Res Bull 34:2027–2034
21. Singman D (1966) J Electrochem Soc 113:502–504
22. Yoshida H, Deguchi H, Miura K, Horiuchi M, Inagaki T (2001) Solid State Ionics 140:191–199
23. Mori T, Drennan J, Lee JH, Li JG, Ikegami T (2002) Solid State Ionics 154–155:461–466
24. Pérez-Coll D, Marrero-Lopez D, Núñez P, Piñol S, Frade JR (2006) Electrochim Acta 51:6463–6469
25. Pikalova EY, Murashkina AA, Maragou VI, Demin AK, Strekalovsky VN, Tsiakaras PE (2011) Int J Hydrogen Energ 36:6175–6183
26. Kleinlogel C, Gauckler LJ (2000) Solid State Ionics 135:567–573
27. Kleinlogel C, Gauckler LJ (2001) Adv Mater 13:1081–1085
28. Zhang TS, Kong LB, Zeng ZQ, Huang HT, Hing P, Xia ZT, Kilner J (2003) J Solid State Electrochem 7:348–354
29. Zhang TS, Ma J, Chan SH, Kilner JA (2005) Solid State Ionics 176:377–384
30. Fagg DP, Kharton VV, Frade JR (2004) J Solid State Electrochem 8:618–625

31. Zhang TS, Ma J, Leng YJ, Chan SH, Hing P, Kilner JA (2004) Solid State Ionics 168:187–195
32. Pérez-Coll D, Núñez P, Abrantes JCC, Fagg DP, Kharton VV, Frade JR (2005) Solid State Ionics 176:2799–2805
33. Bronin DI, Kuzin BL, Yaroslavtsev IY, Bogdanovich NM (2006) J Solid State Electrochem 10:651–658
34. Bi ZH, Cheng MJ, Dong YL, Wu HJ, She YC, Yi BL (2005) Solid State Ionics 176:655–661
35. Polini R, Pamio A, Traversa E (2004) J Eur Ceram Soc 24:1365–1370
36. Majewski P, Rozumek M, Schluckwerder H, Aldinger F (2001) J Am Ceram Soc 84:1093–1096
37. Rozumek M, Majewski P, Sauter L, Aldinger F (2003) J Am Ceram Soc 86:1940–1946
38. Datta P, Majewski P, Aldinger F (2007) Mater Chem Phys 102:240–244
39. Pérez-Coll D, Sánchez-López E, Mather GC (2010) Solid State Ionics 181:1033–1042
40. Ishihara T, Shibayama T, Nishiguchi H, Takita Y (2001) J Mater Sci 36:1125–1131